Proton Structure from the Measurement of 2S-2P Transition Frequencies of Muonic Hydrogen

Aldo Antognini,[1,2]* François Nez,[3] Karsten Schuhmann,[2,4] Fernando D. Amaro,[5] François Biraben,[3] João M. R. Cardoso,[5] Daniel S. Covita,[5,6] Andreas Dax,[7] Satish Dhawan,[7] Marc Diepold,[1] Luis M. P. Fernandes,[5] Adolf Giesen,[4,8] Andrea L. Gouvea,[5] Thomas Graf,[8] Theodor W. Hänsch,[1,9] Paul Indelicato,[3] Lucile Julien,[3] Cheng-Yang Kao,[10] Paul Knowles,[11] Franz Kottmann,[2] Eric-Olivier Le Bigot,[3] Yi-Wei Liu,[10] José A. M. Lopes,[5] Livia Ludhova,[11] Cristina M. B. Monteiro,[5] Françoise Mulhauser,[11] Tobias Nebel,[1] Paul Rabinowitz,[12] Joaquim M. F. dos Santos,[5] Lukas A. Schaller,[11] Catherine Schwob,[3] David Taqqu,[13] João F. C. A. Veloso,[6] Jan Vogelsang,[1] Randolf Pohl[1]

Accurate knowledge of the charge and Zemach radii of the proton is essential, not only for understanding its structure but also as input for tests of bound-state quantum electrodynamics and its predictions for the energy levels of hydrogen. These radii may be extracted from the laser spectroscopy of muonic hydrogen (μp, that is, a proton orbited by a muon). We measured the $2S^{F=0}_{1/2}$-$2P^{F=1}_{3/2}$ transition frequency in μp to be 54611.16(1.05) gigahertz (numbers in parentheses indicate one standard deviation of uncertainty) and reevaluated the $2S^{F=1}_{1/2}$-$2P^{F=2}_{3/2}$ transition frequency, yielding 49881.35(65) gigahertz. From the measurements, we determined the Zemach radius, r_Z = 1.082(37) femtometers, and the magnetic radius, r_M = 0.87(6) femtometer, of the proton. We also extracted the charge radius, r_E = 0.84087(39) femtometer, with an order of magnitude more precision than the 2010-CODATA value and at 7σ variance with respect to it, thus reinforcing the proton radius puzzle.

As the simplest of all stable atoms, hydrogen (H) is unique in its use for comparison between theory and experiment of bound-state energy level structures. Observation of the simple Balmer series in the H emission spectrum inspired the Bohr atomic model and quantum mechanics. More precise measurements of the first Balmer line revealed a splitting of the $n = 2$ states (n is the principal quantum number) arising from the electron's magnetic moment (spin-orbit interaction). Such data represented the crucial validation of the Dirac equation. However, further direct investigation of the hydrogen $2S_{1/2}$-$2P_{1/2}$ energy splitting (Lamb shift) and the 1S hyperfine splitting (HFS) in 1947 by means of microwave spectroscopy revealed a small deviation from the prediction of the Dirac equation. This fueled the development of quantum electrodynamics (QED). Precision measurements of H transition frequencies have been pursued in the past 40 years by laser spectroscopy. In spite of the considerable advances in both experimental (spectroscopy) and theoretical (bound-state QED) accuracy, the comparison between theory and experiment has been hampered by the lack of accurate knowledge of the proton charge and magnetization distributions. The proton structure is important because an electron in an S state has a nonzero probability to be inside the proton. The attractive force between the proton and the electron is thereby reduced because the electric field inside the charge distribution is smaller than the corresponding field produced by a point charge. Thus, the measured transition frequencies depend on the proton size.

Although the shifts of the energy levels associated with the proton finite size are small, it is the 1 to 2% relative uncertainty of the proton charge radius, r_E (*1*–*3*), and Zemach radius, r_Z (*4*, *5*), respectively, that presently limit the theoretical predictions of the Lamb shift and the HFS in H. The Zemach radius reflects the spatial distribution of magnetic moments smeared out (convoluted) by the charge distribution of the proton.

Historically, these radii were derived from measurements of the differential cross section in elastic electron-proton scattering. An independent and more precise determination of these radii can be achieved by laser spectroscopy of the exotic "muonic hydrogen" atom, μp (*6*). Such atoms are formed by a proton and a negative muon, μ^-, a particle whose mass, m_μ, is 207 times that of the electron, m_e. Its atomic energy levels are affected by the finite size of the proton charge distribution (neglecting higher moments of the charge distribution and higher orders in α) by

$$\Delta E_{\text{finite size}} = \frac{2\pi Z\alpha}{3} r_E^2 |\Psi(0)|^2 \qquad (1)$$

where $\Psi(0)$ is the atomic wave function at the origin, α the fine structure constant, and $Z = 1$ the proton charge. For S states, $|\Psi(0)|^2$ is proportional to m_r^3, with $m_r \approx 186 m_e$ being the reduced mass of the μp system. The muon Bohr radius is 186 times smaller than the electron Bohr radius in H, resulting in a strongly increased sensitivity of μp to the proton finite size.

We have recently performed the measurement of the $2S^{F=1}_{1/2}$-$2P^{F=2}_{3/2}$ transition (Fig. 1 C) in μp, which led to a determination of r_E with a relative accuracy $u_r = 8 \times 10^{-4}$ (*6*). Yet the r_E value obtained is seven standard deviations smaller than the world average (*7*) based on H spectroscopy and elastic electron scattering. This discrepancy has triggered a lively discussion addressing the accuracy of these experiments, bound-state QED, the proton structure, the Rydberg constant (R_∞), and possibilities of new physics.

Principle and measurements. The principle of the muonic hydrogen Lamb shift experiment is to form muonic hydrogen in the 2S state (Fig. 1A) and then measure the 2S-2P energy splitting (Fig. 1C) by means of laser spectroscopy (Fig. 1B) using the setup sketched in Fig. 2 (*6*).

Negative muons from the proton accelerator of the Paul Scherrer Institute, Switzerland, are stopped in H_2 gas at 1 hPa and 20°C, where highly excited μp atoms ($n \approx 14$) are formed. Most of these deexcite quickly to the 1S ground state (*8*), but ~1% populate the long-lived 2S state (Fig. 1A), whose lifetime is ~1 μs at 1 hPa (*9*). A 5-ns laser pulse with a wavelength tunable from 5.5 to 6 μm (*10*, *11*) illuminates the target gas volume, about 0.9 μs after the muon reached the target. On-resonance light induces 2S → 2P transitions, which are immediately followed by 2P → 1S deexcitation via 1.9-keV K_α x-ray emission (lifetime τ_{2P} = 8.5 ps). A resonance curve is obtained by measuring the number of 1.9-keV x-rays in time coincidence with the laser pulse (i.e., within a time window of 0.900 to 0.975 μs after the muon entry into the target) as a function of the laser wavelength. The 75-ns width of this window corresponds to the confinement time of the laser light within the multipass mirror cavity surrounding the gas target.

We have measured the two 2S-2P transitions depicted in Fig. 1C, one from the singlet state with frequency $\nu_s = \nu(2S^{F=0}_{1/2} - 2P^{F=1}_{3/2})$ and wavelength $\lambda_s \cong 5.5$ μm and the other from the triplet state with $\nu_t = \nu(2S^{F=1}_{1/2} - 2P^{F=2}_{3/2})$ and $\lambda_t \cong 6.0$ μm. For the latter, we present an updated analysis of the data presented in (*6*).

[1]Max-Planck-Institut für Quantenoptik, 85748 Garching, Germany. [2]Institute for Particle Physics, Eidgenössische Technische Hochschule (ETH) Zürich, 8093 Zürich, Switzerland. [3]Laboratoire Kastler Brossel, École Normale Supérieure, CNRS and Université Pierre et Marie Curie (UPMC), 75252 Paris, CEDEX 05, France. [4]Dausinger and Giesen GmbH, Rotebühlstraße 87, 70178 Stuttgart, Germany. [5]Departamento de Física, Universidade de Coimbra, 3004-516 Coimbra, Portugal. [6]I3N, Departamento de Física, Universidade de Aveiro, 3810-193 Aveiro, Portugal. [7]Physics Department, Yale University, New Haven, CT 06520–8121, USA. [8]Institut für Strahlwerkzeuge, Universität Stuttgart, 70569 Stuttgart, Germany. [9]Ludwig-Maximilians-Universität, Munich, Germany. [10]Physics Department, National Tsing Hua University, Hsinchu 300, Taiwan. [11]Département de Physique, Université de Fribourg, 1700 Fribourg, Switzerland. [12]Department of Chemistry, Princeton University, Princeton, NJ 08544–1009, USA. [13]Paul Scherrer Institute, 5232 Villigen-PSI, Switzerland.

*To whom correspondence should be addressed. E-mail: aldo@phys.ethz.ch

Figure 3 shows the two measured μp resonances. Details of the data analysis are given in (*12*). The laser frequency was changed every few hours, and we accumulated data for up to 13 hours per laser frequency. The laser frequency was calibrated [supplement in (*6*)] by using well-known water absorption lines. The resonance positions corrected for laser intensity effects using the line shape model (*12*) are

$$\nu_s = 54611.16(1.00)^{stat}(30)^{sys}\,\mathrm{GHz} \quad (2)$$

$$\nu_t = 49881.35(57)^{stat}(30)^{sys}\,\mathrm{GHz} \quad (3)$$

where "stat" and "sys" indicate statistical and systematic uncertainties, giving total experimental uncertainties of 1.05 and 0.65 GHz, respectively. Although extracted from the same data, the frequency value of the triplet resonance, ν_t, is slightly more accurate than in (*6*) owing to several improvements in the data analysis. The fitted line widths are 20.0(3.6) and 15.9(2.4) GHz, respectively, compatible with the expected 19.0 GHz resulting from the laser bandwidth (1.75 GHz at full width at half maximum) and the Doppler broadening (1 GHz) of the 18.6-GHz natural line width.

The systematic uncertainty of each measurement is 300 MHz, given by the frequency calibration uncertainty arising from pulse-to-pulse fluctuations in the laser and from broadening effects occurring in the Raman process. Other systematic corrections we have considered are the Zeeman shift in the 5-T field (<60 MHz), AC and DC Stark shifts (<1 MHz), Doppler shift (<1 MHz), pressure shift (<2 MHz), and black-body radiation shift (<<1 MHz). All these typically important atomic spectroscopy systematics are small because of the small size of μp.

The Lamb shift and the hyperfine splitting. From these two transition measurements, we can independently deduce both the Lamb shift ($\Delta E_L = \Delta E_{2P_{1/2}-2S_{1/2}}$) and the 2S-HFS splitting (ΔE_{HFS}) by the linear combinations (*13*)

$$\frac{1}{4}h\nu_s + \frac{3}{4}h\nu_t = \Delta E_L + 8.8123(2)\mathrm{meV}$$

$$h\nu_s - h\nu_t = \Delta E_{HFS} - 3.2480(2)\mathrm{meV} \quad (4)$$

Finite size effects are included in ΔE_L and ΔE_{HFS}. The numerical terms include the calculated values of the 2P fine structure, the $2P_{3/2}$ hyperfine splitting, and the mixing of the 2P states (*14*–*18*). The finite proton size effects on the 2P fine and hyperfine structure are smaller than 1×10^{-4} meV because of the small overlap between the 2P wave functions and the nucleus. Thus, their uncertainties arising from the proton structure are negligible. By using the measured transition frequencies ν_s and ν_t in Eqs. 4, we obtain (1 meV corresponds to 241.79893 GHz)

$$\Delta E_L^{exp} = 202.3706(23)\ \mathrm{meV} \quad (5)$$

$$\Delta E_{HFS}^{exp} = 22.8089(51)\ \mathrm{meV} \quad (6)$$

The uncertainties result from quadratically adding the statistical and systematic uncertainties of ν_s and ν_t.

The charge radius. The theory (*14*, *16*–*22*) relating the Lamb shift to r_E yields (*13*):

$$\Delta E_L^{th} = 206.0336(15) - 5.2275(10)r_E^2 + \Delta E_{TPE} \quad (7)$$

where E is in meV and r_E is the root mean square (RMS) charge radius given in fm and defined as $r_E^2 = \int d^3r\, r^2\, \rho_E(\boldsymbol{r})$ with ρ_E being the normalized proton charge distribution. The first term on the right side of Eq. 7 accounts for radiative, relativistic, and recoil effects. Fine and hyperfine corrections are absent here as a consequence of Eqs. 4. The other terms arise from the proton structure. The leading finite size effect $-5.2275(10)r_E^2$ meV is approximately given by Eq. 1 with corrections given in (*13*, *17*, *18*). Two-photon exchange (TPE) effects, including the proton polarizability, are covered by the term $\Delta E_{TPE} = 0.0332(20)$ meV (*19*, *24*–*26*). Issues related with TPE are discussed in (*12*, *13*).

The comparison of ΔE_L^{th} (Eq. 7) with ΔE_L^{exp} (Eq. 5) yields

$$r_E = 0.84087(26)^{exp}(29)^{th}\ \mathrm{fm} = 0.84087(39)\ \mathrm{fm} \quad (8)$$

This r_E value is compatible with our previous μp result (*6*), but 1.7 times more precise, and is now independent of the theoretical prediction of the 2S-HFS. Although an order of magnitude more precise, the μp-derived proton radius is at 7σ variance with the CODATA-2010 (*7*) value of $r_E = 0.8775(51)$ fm based on H spectroscopy and electron-proton scattering.

Magnetic and Zemach radii. The theoretical prediction (*17*, *18*, *27*–*29*) of the 2S-HFS is (*13*)

$$\Delta E_{HFS}^{th} = 22.9763(15) - 0.1621(10)r_Z + \Delta E_{HFS}^{pol} \quad (9)$$

where E is in meV and r_Z is in fm. The first term is the Fermi energy arising from the interaction between the muon and the proton magnetic moments, corrected for radiative and recoil contributions, and includes a small dependence of $-0.0022r_E^2$ meV = −0.0016 meV on the charge radius (*13*).

The leading proton structure term depends on r_Z, defined as

$$r_Z = \int d^3r \int d^3r' r' \rho_E(\boldsymbol{r}) \rho_M(\mathbf{r} - \mathbf{r}') \quad (10)$$

with ρ_M being the normalized proton magnetic moment distribution. The HFS polariz-

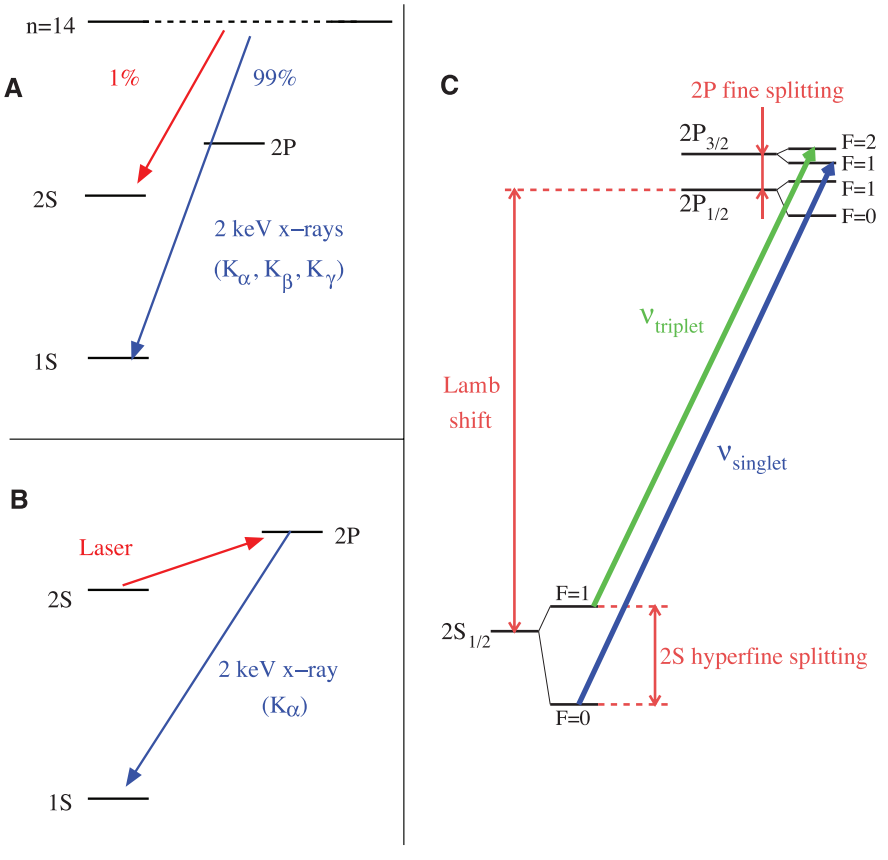

Fig. 1. (**A**) Formation of μp in highly excited states and subsequent cascade with emission of "prompt" $K_{\alpha,\beta,\gamma}$. (**B**) Laser excitation of the 2S-2P transition with subsequent decay to the ground state with K_α emission. (**C**) 2S and 2P energy levels. The measured transitions ν_s and ν_t are indicated together with the Lamb shift, 2S-HFS, and 2P-fine and hyperfine splitting.

ability contribution $\Delta E_{\mathrm{HFS}}^{\mathrm{pol}} = 0.0080(26)$ meV is evaluated by using measured polarized structure functions (*28*, *29*).

Comparison of $\Delta E_{\mathrm{HFS}}^{\mathrm{th}}$ (Eq. 9) with $\Delta E_{\mathrm{HFS}}^{\mathrm{exp}}$ (Eq. 6) yields

$$r_Z = 1.082(31)^{\mathrm{exp}}(20)^{\mathrm{th}}\ \mathrm{fm} = 1.082(37)\ \mathrm{fm} \quad (11)$$

This value has a relative accuracy of $u_r = 3.4\%$, limited by our measurements, and is compatible with both $r_Z = 1.086(12)$ fm (*4*) and $r_Z = 1.045(4)$ fm (*5*) from electron-proton scattering and $r_Z = 1.047(16)$ fm (*30*) and $r_Z = 1.037(16)$ fm (*31*) from H spectroscopy. The agreement between the muonic and the other r_Z values implies agreement between predicted and measured 2S-HFS.

By knowing r_Z and r_E, it is possible to extract the magnetic RMS radius when models for charge ρ_E and magnetization distributions ρ_M are assumed. Use of a dipole model for both, with the muonic values for r_E and r_Z, yields $r_M = 0.87(6)$ fm, in agreement with recent results from electron scattering $r_M = 0.803(17)$ fm (*1*, *32*), $r_M = 0.867(28)$ fm (*2*), and $r_M = 0.86(3)$ fm (*33*).

The proton-size puzzle. The origin of the large discrepancy between our r_E and the CODATA value is not yet known (*34*). The radius definitions used in H and μp spectroscopy and in scattering are consistent (*35*). Various studies have confirmed the theory of the μp Lamb shift and in particular the proton-structure contributions. The extracted r_E value changes by less than our quoted uncertainty for various models of the proton charge distribution (*36*).

Solving the proton radius puzzle by assuming a large tail for the proton charge distribution (*37*) is ruled out by electron-proton scattering data (*5*, *38*, *39*) and by chiral perturbation theory (*40*). The possibility that we performed spectroscopy on a three-body system such as a *pp*μ-molecule or a μ*pe*-ion instead of a "bare" μp atom (*41*) has been excluded by three-body calculations (*42*).

The ΔE_{TPE} between the muon and a proton with structure is evaluated by using the doubly virtual Compton amplitude, which, by means of dispersion relations, can be related to measured proton form factors and spin-averaged structure functions. Part of a subtraction term needed to remove a divergence in one Compton amplitude is usually approximated by using the one-photon on-shell form factor (*19*). A possible large uncertainty related with this approximation has been emphasized in (*26*, *43*), but this possibility has been strongly constrained by heavy-baryon chiral perturbation theory calculations (*25*).

R_∞ is necessary to extract r_E from the measured 1S-2S transition frequency in H (*44*). Hence, several new atomic physics experiments aim at an improved determination of R_∞, checking also for possible systematic shifts in previous R_∞ determinations in H.

Recent electron-proton scattering measurements yielded $r_E = 0.879(9)$ fm (*1*) and $r_E = 0.875(11)$ fm (*2*), in disagreement with our result. The extraction of r_E from elastic electron-proton scattering requires extrapolation of the measured electric form factor to zero momentum transfer, $Q^2 = 0$. This extrapolation has been investigated in detail (*45*). A global fit of proton and neutron form factors based on dispersion relations and the vector-dominance model gives $r_E = 0.84(1)$ fm (*33*), in agreement with our value, albeit with a larger χ^2 than the phenomenological fits (*1*).

The r_E value from μp could deviate from the values from electron-proton scattering and H spectroscopy if the muon-proton interaction differs from the electron-proton interaction. The window for such "new physics" is small given the multitude of low-energy experimental constraints coming from hydrogen, muonium, and μSi spectroscopy; electron and muon g-2 measurements; meson decays; neutron scattering; and searches for dark photons, etc. [(*46*) and references therein]. Nevertheless, models with new force carriers of MeV-mass have been proposed that could explain the r_E puzzle without conflicting with other experimental observations (*46*, *47*).

Conclusions. We have presented a measurement of the $2S_{1/2}^{F=0}$-$2P_{3/2}^{F=1}$ transition in μp and a reanalysis of the $2S_{1/2}^{F=1}$-$2P_{3/2}^{F=2}$ transition (*6*). Summing and subtracting these two measurements leads to an independent assessment of the 2S-HFS

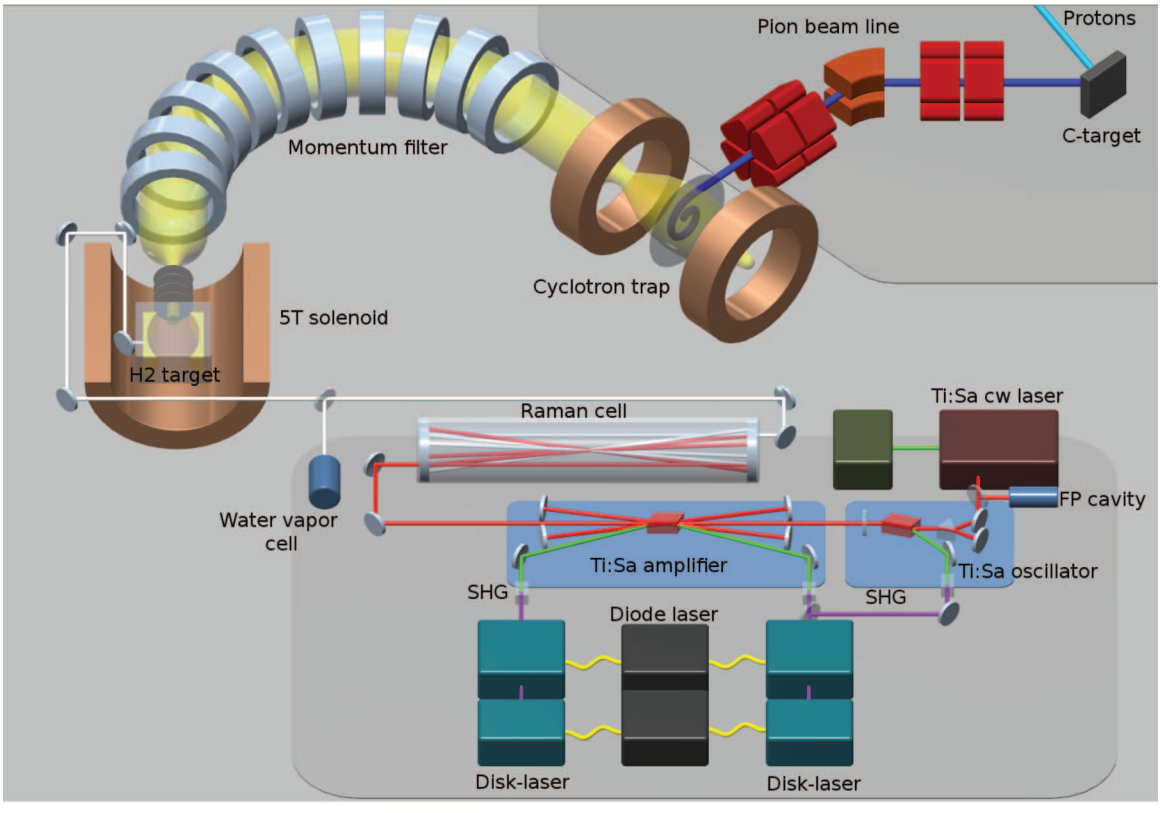

Fig. 2. Experimental apparatus. Accelerator-created negative pions are transported to the cyclotron trap. Here they decay into MeV-energy muons, which are decelerated by a thin foil placed at the trap center. The resulting keV-energy muons leave the trap and follow a toroidal magnetic field of 0.15 T (acting as a momentum filter) before entering a 5-T solenoid where the hydrogen target is placed. A muon entrance detector provides a signal that triggers the laser system. About 0.9 μs later, the formed μp is irradiated by the laser pulse to induce the 2S-2P transition. Such a short delay is achieved by the continuous 1.5-kW pumping of two Q-switched disk lasers operating in prelasing mode (*8*). The disk-laser pulses are frequency doubled [second harmonic generation (SHG)] and used to pump a Ti:Sa laser. The Ti:Sa oscillator is seeded by a stabilized continuous-wave Ti:Sa laser, and the emitted red pulses of ~700-nm wavelength and 5-ns length are well suited for efficient Raman conversion to 5.5 - 6 μm via three Stokes shifts in hydrogen gas at 15 bar (*9*). These pulses are then injected into a multipass cavity surrounding the hydrogen gas target. Absolute calibration from 5.5 to 6 μm was performed by water vapor spectroscopy.

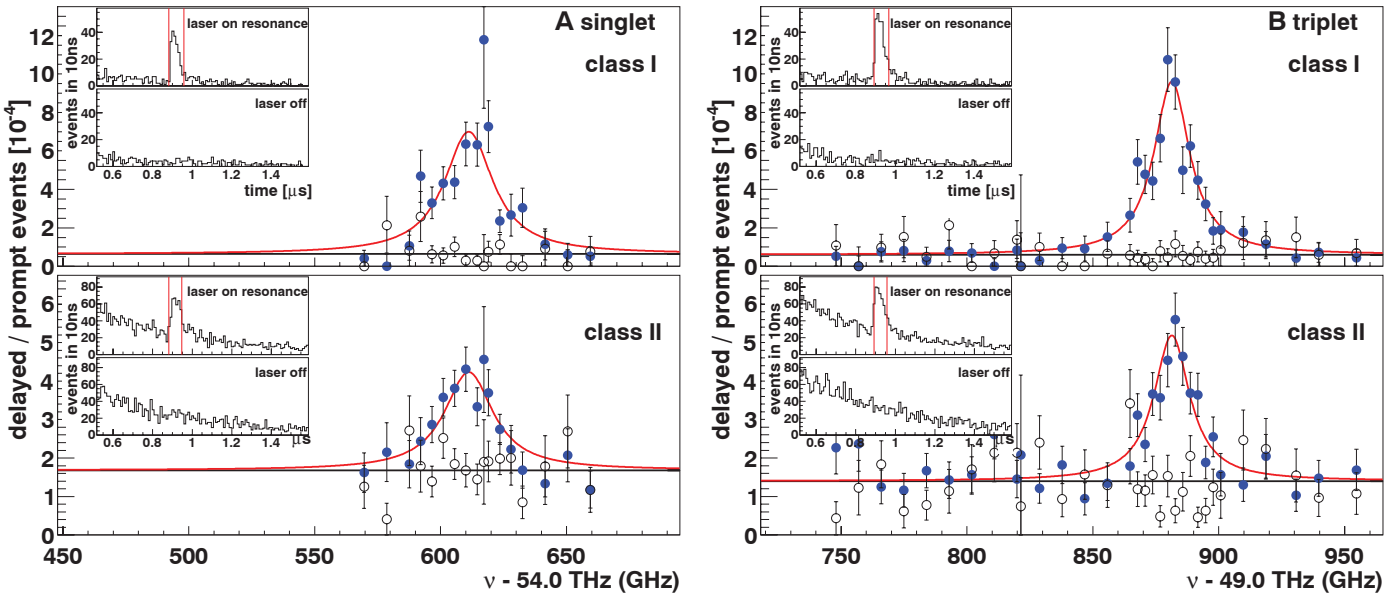

Fig. 3. Muonic hydrogen resonances (solid circles) for singlet ν_s (**A**) and triplet ν_t (**B**) transitions. Open circles show data recorded without laser pulses. Two resonance curves are given for each transition to account for two different classes, I and II, of muon decay electrons (*12*). Error bars indicate the standard error. (Insets) The time spectra of K_α x-rays. The vertical lines indicate the laser time window.

and the "pure" 2S-2P Lamb shift. By comparison with theoretical predictions, two proton-structure parameters are determined: $r_E = 0.84087(39)$ fm and $r_Z = 1.082(37)$ fm. These radii play a crucial role in the understanding of the atomic hydrogen spectrum (bound-state QED). They also provide information needed to test quantum chromodynamics in the nonperturbative region.

Subtracting the H(1S) and H(2S) Lamb shifts, computed by using the muonic r_E, from the measured 1S−2S transition frequency in H gives $R_\infty = 3.2898419602495(10)(25) \times 10^{15}$ Hz/c. The first uncertainty of 1.0 kHz/c and the second of 2.5 kHz/c originate from the uncertainties of the muonic r_E and QED theory in H, respectively. This R_∞ deviates by −115 kHz/c, corresponding to 6.6 standard deviations, from the CODATA (*7*) value but is six times more precise (relative accuracy of $u_r = 8 \times 10^{-13}$).

Our value of the proton charge radius $r_E(p)$ can be used to determine a new deuteron charge radius, $r_E(d)$, by using the accurately measured isotope shift of the 1S-2S transition in H and D (*48*). From equation 4 of (*48*)

$$r_E^2(d) - r_E^2(p) = 3.82007(65)\ \text{fm}^2 \quad (12)$$

we obtain a precise value of the deuteron RMS charge radius

$$r_E(d) = 2.12771(22)\ \text{fm} \quad (13)$$

in agreement with $r_E(d) = 2.130(10)$ fm (*49*) from electron-deuteron scattering but more than an order of magnitude more precise. The CODATA (*7*) value $r_E(d) = 2.1424(25)$ fm is in disagreement, because it is dominantly based on the 7σ discrepant $r_E(p)$ value of CODATA combined with Eq. 12. The Lamb shift in muonic deuterium μd can provide an independent $r_E(d)$ value.

References and Notes

1. J. C. Bernauer *et al.*, *Phys. Rev. Lett.* **105**, 242001 (2010).
2. X. Zhan *et al.*, *Phys. Lett. B* **705**, 59 (2011).
3. P. G. Blunden, I. Sick, *Phys. Rev. C Nucl. Phys.* **72**, 057601 (2005).
4. J. Friar, I. Sick, *Phys. Lett. B* **579**, 285 (2004).
5. M. O. Distler, J. C. Bernauer, T. Walcher, *Phys. Lett. B* **696**, 343 (2011).
6. R. Pohl *et al.*, *Nature* **466**, 213 (2010).
7. P. J. Mohr, B. N. Taylor, D. B. Newell, *Rev. Mod. Phys.* **84**, 1527 (2012).
8. R. Pohl, *Hyperfine Interact.* **193**, 115 (2009).
9. R. Pohl *et al.*, *Phys. Rev. Lett.* **97**, 193402 (2006).
10. A. Antognini *et al.*, *IEEE J. Quantum Electron.* **45**, 993 (2009).
11. A. Antognini *et al.*, *Opt. Commun.* **253**, 362 (2005).
12. Materials and methods are available as supplementary materials on *Science* Online.
13. A. Antognini *et al.*, *Ann. Phys.*, published online 31 December 2012 (10.1016/j.aop.2012.12.003).
14. K. Pachucki, *Phys. Rev. A* **53**, 2092 (1996).
15. A. P. Martynenko, *Phys. Atomic Nuclei* **71**, 125 (2008).
16. U. D. Jentschura, *Ann. Phys.* **326**, 500 (2011).
17. E. Borie, *Ann. Phys.* **327**, 733 (2012).
18. E. Borie, http://arxiv.org/abs/1103.1772v6 (2012).
19. K. Pachucki, *Phys. Rev. A* **60**, 3593 (1999).
20. M. I. Eides, H. Grotch, V. A. Shelyuto, *Phys. Rep.* **342**, 63 (2001).
21. S. G. Karshenboim, E. Y. Korzinin, V. G. Ivanov, V. A. Shelyuto, *JETP Lett.* **92**, 8 (2010).
22. S. G. Karshenboim, V. G. Ivanov, E. Y. Korzinin, *Phys. Rev. A* **85**, 032509 (2012).
23. U. D. Jentschura, *Phys. Rev. A* **84**, 012505 (2011).
24. C. E. Carlson, M. Vanderhaeghen, *Phys. Rev. A* **84**, 020102 (2011).
25. M. C. Birse, J. A. McGovern, *Eur. Phys. J. A* **48**, 120 (2012).
26. R. J. Hill, G. Paz, *Phys. Rev. Lett.* **107**, 160402 (2011).
27. A. P. Martynenko, *Phys. Rev. A* **71**, 022506 (2005).
28. C. E. Carlson, V. Nazaryan, K. Griffioen, *Phys. Rev. A* **83**, 042509 (2011).
29. E. Cherednikova, R. Faustov, A. Martynenko, *Nucl. Phys. A.* **703**, 365 (2002).
30. A. V. Volotka, V. M. Shabaev, G. Plunien, G. Soff, *Eur. Phys. J. D* **33**, 23 (2005).
31. A. Dupays, A. Beswick, B. Lepetit, C. Rizzo, D. Bakalov, *Phys. Rev. A* **68**, 052503 (2003).
32. J. C. Bernauer *et al.*, *Phys. Rev. Lett.* **107**, 119102 (2011).
33. I. T. Lorenz, H.-W. Hammer, U. Meißner, *Eur. Phys. J. A* **48**, 151 (2012).
34. R. Pohl, R. Gilman, G. A. Miller, K. Pachucki, http://arxiv.org/abs/1301.0905 (2013).
35. U. D. Jentschura, *Eur. Phys. J. D* **61**, 7 (2011).
36. J. D. Carroll, A. W. Thomas, J. Rafelski, G. A. Miller, http://arxiv.org/abs/1108.2541v1 (2011).
37. A. De Rújula, *Phys. Lett. B* **697**, 26 (2011).
38. J. L. Friar, I. Sick, *Phys. Rev. A* **72**, 040502 (2005).
39. I. C. Cloët, G. A. Miller, *Phys. Rev. C Nucl. Phys.* **83**, 012201(R) (2011).
40. A. Pineda, *Phys. Rev. C Nucl. Phys.* **71**, 065205 (2005).
41. U. D. Jentschura, *Ann. Phys.* **326**, 516 (2011).
42. J.-P. Karr, L. Hilico, *Phys. Rev. Lett.* **109**, 103401 (2012).
43. G. A. Miller, A. W. Thomas, J. D. Carroll, J. Rafelski, *Phys. Rev. A* **84**, 020101(R) (2011).
44. C. G. Parthey *et al.*, *Phys. Rev. Lett.* **107**, 203001 (2011).
45. R. J. Hill, G. Paz, *Phys. Rev. D* **82**, 113005 (2010).
46. C. E. Carlson, B. C. Rislow, *Phys. Rev. D* **86**, 035013 (2012).
47. B. Batell, D. McKeen, M. Pospelov, *Phys. Rev. Lett.* **107**, 011803 (2011).
48. C. G. Parthey *et al.*, *Phys. Rev. Lett.* **104**, 233001 (2010).
49. I. Sick, D. Trautmann, *Nucl. Phys. A.* **637**, 559 (1998).

Acknowledgments: We thank L. M. Simons, B. Leoni, H. Brückner, K. Linner, W. Simon, J. Alpstäg, Z. Hochman, N. Schlumpf, U. Hartmann, S. Ritt, M. Gaspar, M. Horisberger, B. Weichelt, J. Früchtenicht, A. Voss, M. Larionov, F. Dausinger, and K. Kirch for their contributions. We acknowledge support from the Max Planck Society and the Max Planck Foundation, the Swiss National Science Foundation (projects 200020-100632 and 200021L-138175/1), the Swiss Academy of Engineering Sciences, the Bonus Qualité Recherche de l'Unités de Formations et de Recherche de physique fondamentale et appliquée de l'UPMC, the program PAI Germaine de Staël no. 07819NH du ministère des affaires étrangères France, the Ecole Normale Supérieure (ENS), UPMC, CNRS, and the Fundação para a Ciência e a Tecnologia (FCT, Portugal) and Fundo Europeu De Desenvolvimento Regional (project PTDC/FIS/102110/2008 and grant SFRH/BPD/46611/2008). P.I. acknowledges support by the ExtreMe Matter Institute, Helmholtz Alliance HA216/EMMI. T.N. and R.P. were in part supported by the European Research Council (ERC) Starting Grant no. 279765. A.L.G. received support from FCT through program grant SFRH/BD/66731/2009.

Supplementary Materials

www.sciencemag.org/cgi/content/full/339/6118/417/DC1
Materials and Methods
Supplementary Text
References

11 September 2012; accepted 30 November 2012
10.1126/science.1230016

Science
AAAS

Proton Structure from the Measurement of 2S-2P Transition Frequencies of Muonic Hydrogen

Aldo Antognini, François Nez, Karsten Schuhmann, Fernando D. Amaro, François Biraben, João M. R. Cardoso, Daniel S. Covita, Andreas Dax, Satish Dhawan, Marc Diepold, Luis M. P. Fernandes, Adolf Giesen, Andrea L. Gouvea, Thomas Graf, Theodor W. Hänsch, Paul Indelicato, Lucile Julien, Cheng-Yang Kao, Paul Knowles, Franz Kottmann, Eric-Olivier Le Bigot, Yi-Wei Liu, José A. M. Lopes, Livia Ludhova, Cristina M. B. Monteiro, Françoise Mulhauser, Tobias Nebel, Paul Rabinowitz, Joaquim M. F. dos Santos, Lukas A. Schaller, Catherine Schwob, David Taqqu, João F. C. A. Veloso, Jan Vogelsang and Randolf Pohl (January 24, 2013)
Science **339** (6118), 417-420. [doi: 10.1126/science.1230016]

Editor's Summary

Proton Still Too Small

Despite a proton's tiny size, it is possible to measure its radius based on its charge or magnetization distributions. Traditional measurements of proton radius were based on the scattering between protons and electrons. Recently, a precision measurement of a line in the spectrum of muonium ––an atom consisting of a proton and a muon, instead of an electron––revealed a radius inconsistent with that deduced from scattering studies. **Antognini *et al.*** (p. 417; see the Perspective by **Margolis**) examined a different spectral line of muonium, with results less dependent on theoretical analyses, yet still inconsistent with the scattering result; in fact, the discrepancy increased.

Science (print ISSN 0036-8075; online ISSN 1095-9203) is published weekly, except the last week in December, by the American Association for the Advancement of Science, 1200 New York Avenue NW, Washington, DC 20005.